

---

# Learning to Scan: A Deep Reinforcement Learning Approach for Personalized Scanning in CT Imaging

---

**Ziju Shen\***

Academy for Advanced Interdisciplinary Studies  
Peking University  
zjshen@pku.edu.cn

**Yufei Wang\***

Computer Science Department  
Carnegie Mellon University  
yufeiw2@andrew.cmu.edu

**Dufan Wu**

Center for Advanced Medical Computing and Analysis  
Massachusetts General Hospital and Harvard Medical School  
dwu6@mgh.harvard.edu

**Xu Yang**

Department of Mathematics  
University of California, Santa Barbara  
xuyang@math.ucsb.edu

**Bin Dong**

Beijing International Center for Mathematical Research  
Institute for Artificial Intelligence  
Center for Data Science  
Peking University  
dongbin@math.pku.edu.cn

## Abstract

Computed Tomography (CT) takes X-ray measurements on the subjects to reconstruct tomographic images. As X-ray is radioactive, it is desirable to control the total amount of dose of X-ray for safety concerns. Therefore, we can only select a limited number of measurement angles and assign each of them limited amount of dose. Traditional methods such as compressed sensing usually randomly select the angles and equally distribute the allowed dose on them. In most CT reconstruction models, the emphasize is on designing effective image representations, while much less emphasize is on improving the scanning strategy. The simple scanning strategy of random angle selection and equal dose distribution performs well in general, but they may not be ideal for each individual subject. It is more desirable to design a personalized scanning strategy for each subject to obtain better reconstruction result. In this paper, we propose to use Reinforcement Learning (RL) to learn a personalized scanning policy to select the angles and the dose at each chosen angle for each individual subject. We first formulate the CT scanning process as an MDP, and then use modern deep RL methods to solve it. The learned personalized scanning strategy not only leads to better reconstruction results, but also shows strong generalization to be combined with different reconstruction algorithms.

---

\*Equal Contribution

# 1 Introduction

X-ray based computed tomography (CT) is a medical imaging procedure that reconstructs tomographic images by taking X-ray measurements from different angles. To obtain high-quality reconstructions, in early reconstruction algorithms such as FBP [1] and ART [2], a number of different angles need to be measured. However, since X-ray is radioactive, the total dose of X-ray needs to be restricted in the scanning process, and thus we need to either decrease the X-ray intensity at each chosen angle, or to reduce the total number of angles taken. Decreasing X-ray intensity in each angle will result in more noisy measurements, while fewer angles will reduce the information we need for a high-quality reconstruction. This causes great challenge in designing efficient and effective reconstruction algorithms.

Compressed sensing [3] resolves the issue to a certain extent. According to the theory of compressed sensing, if an image has a sparse property after certain transformations (e.g., wavelet transform), then it can be robustly reconstructed with a reduced number of random measurements by solving an  $l_1$ -minimization problem when the measurements and the transformation satisfy the D-RIP condition [4]. We can use the alternating direction method of multipliers (ADMM) [5, 6, 7] or primal-dual hybrid gradient method (PDHG) [8, 9, 10] to solve this  $l_1$ -minimization problem to obtain a reconstructed image.

In the literature of CT image reconstruction or image restoration in general, people are focused on designing effective regularizations, which includes the total variation (TV) [11], nonlocal means [12], BM3D [13], WNNM [14], wavelets and wavelet frame models [15, 16, 17], K-SVD [18], data-driven (tight) frame [19, 20], low dimensional manifold method (LDMM) [21], etc. More recently, the rapid development of machine learning, especially deep learning, has lead to a paradigm shift of modeling and algorithmic design in computer vision and medical imaging [22, 23, 24, 25, 26]. Deep learning based models are able to leverage large image datasets to learn better image representations and produce better image reconstruction results than traditional methods [27, 28, 29, 30, 31].

In most CT reconstruction models, the emphasize is on designing effective image representation, while much less emphasize is on improving the scanning strategy. In compressed sensing, the scanning strategy is entirely random [32, 4], i.e., the measurement angles are selected randomly and the dose are allocated uniformly across the angles. In general, such a random scanning strategy, i.e., random angle selection and uniform dose allocation, performs well in practice. However, for each individual subject, this random scanning strategy may not be ideal. It is more desirable to design a personalized scanning strategy for each subject to achieve better reconstruction results. Our key observation is that the measurements collected in the early stage during the scanning process can be used to guide the later scanning.

Despite the potential improvement of a personalized scanning strategy for each individual subject, it is very difficult to handcraft such a strategy by a human expert. This is where machine learning can help. The personalized scanning strategy can be learned using either active learning [33] or Reinforcement Learning (RL) [34]. In this paper, we propose to use reinforcement learning to learn such a personalized scanning strategy for each subject. The reason we choose RL over active learning is that RL is non-greedy and naturally guarantees the long-term reconstruction quality. We formulate the CT scanning process as a Markov Decision Process (MDP), where the state includes currently collected measurements, the action determines the next measurement angle and the dose usage, and the reward depends on the reconstruction quality. We further use modern Deep RL algorithms to solve it. We show in the experiments that the personalized scanning policy learned by RL significantly outperforms the random scanning strategy in terms of the reconstruction quality, and can generalize to be combined with different reconstruction algorithms. To the best of our knowledge, we are the first to use Deep RL to learn a personalized CT scanning strategy.

## 1.1 Related works

For compressed sensing, there have been two primary categories of scanning strategies: static and dynamic. Static scanning strategy refers to the method which collects measurements in a fixed order. Low-discrepancy sampling [35] and uniformly spaced sparse sampling methods [36] are two examples of static scanning strategy. Non-uniform static scanning strategy based on the model of the subject to be scanned is proposed in [37, 38]. However, because the order of measurements is

predetermined, static scanning strategy is not flexible for different subjects and may lead to poor results for some of them.

Dynamic scanning strategy refers to the methods which collect measurement adaptively based on information obtained from previous measurements. One traditional method tries to find the most suitable measurements which can minimize the entropy to decrease uncertainty of images, such as BCS [39, 40]. Similarly, other methods [41, 42, 43] use the information gain at each additional scan to guide the selection of the next measurement. However, these methods are typically greedy methods in nature, have many hyperparameters to be properly tuned, and are slow during inference as they either need to take inverse of large matrices, or to run the reconstruction algorithm for many times when determining the best next angle. More recently, deep neural networks are used to estimate the expected reduction in distortion (ERD) in the reconstructed image when an additional measurement is selected [44, 45, 46, 47, 48, 49]. However, for the estimate of ERD to be accurate, it requires a large number of measurements in training.

All the above methods are not specific to CT scanning. They are greedy in nature and do not provide a strategy for dose allocation. In contrast, RL is able to generate a non-greedy policy that aims at maximizing long-term rewards. Furthermore, the setting of RL is flexible enough to handle both angle selection and dose allocation, and even more decision options during scanning. Therefore, in this paper we use RL to design a scanning policy that acts optimally on each individual subject. In Scanning Transmission Electron Microscopy (STEM), a recent work by [50] proposes to use RL to guide the movement of the detector and uses a generator to generate reconstructed images. However, since the image modality is drastically different from CT, the proposed MDP (especially the state, action and architecture of the policy network) is vastly different from what is proposed in this paper.

## 2 Preliminaries

### 2.1 CT Reconstruction

Let  $f \in \mathbb{R}^n$  denote the discretised image of a subject, with  $n$  being the number of pixels. The scanning process is a linear operation which can be described as a matrix  $A \in \mathbb{R}^{m \times n}$ . Different scanning angles lead to different forms of linear operators  $A$ . The measurements  $p \in \mathbb{R}^m$  can be expressed as

$$p = Af + \epsilon, \quad (1)$$

where  $\epsilon$  is an additive noise. The reconstruction process is to reconstruct the CT image  $f$  from the measurements  $p$ . As equation (1) is a linear equation, it can be directly solved by ART or SART algorithm [2, 51]. However, as  $m$  can be far smaller than  $n$ , equation (1) has far less equations than unknowns. In order to obtain high-quality solutions, regularization-based models are often used, which typically take the form as follows:

$$\min_f \frac{1}{2} \|p - Af\|_2^2 + \lambda R(f), \quad (2)$$

where  $R(f)$  is the regularization term. Two benchmarking regularization terms are TV regularization  $R(f) = \|\nabla f\|_1$  [52] and wavelet regularization  $R(f) = \|Wf\|_1$  [53], where  $W$  is the wavelet transform. Both of these two optimization problems can be solved by ADMM or PDHG.

### 2.2 Relationship between Measurement Noise and Dose

Noise intensity on measurements heavily relies on the X-ray dose. It is common to assume that the measurement noise follows a Gaussian distribution [54],  $\epsilon \sim \mathcal{N}(0, \sigma)$ , and

$$\sigma \propto \frac{1}{\sqrt{n_{\max} d \exp(-P)}}, \quad (3)$$

where  $d$  is the X-ray dose used in a measurement,  $P$  is the average intensity of measurement, and  $n_{\max}$  is the maximum number of photons the source can generate. We can easily see that if we use more dose, the noise level becomes smaller.

## 2.3 Some Further Discussions

As equation (1) shows, the measurements we obtain from a CT scan depends both on the angle (which determines  $A$ ), and the X-ray dose (which determines  $\epsilon$ ). Due to the limitation on X-ray dose usage, we can only select a limited number of angles and assign each of them limited amount of dose. Traditional methods simply randomly select the angles and equally distribute the allowed dose on them. Our goal is to use RL to learn a personalized policy to select the angles and the dose at each chosen angle for each individual subject.

## 3 Method

Our goal is to learn a policy that can decide the next measurement angle and its corresponding X-ray dose based on the measurements that we have already obtained in the scanning process. We now present how the scanning process can be formulated as a Markov Decision Process (MDP) and solved by reinforcement learning algorithms. We choose the Proximal Policy Optimization (PPO) method as our RL algorithm [55].

### 3.1 A Brief Review on MDP and PPO

MDP is a tuple  $(\mathcal{S}, \mathcal{A}, \gamma, \mathbb{P}, r)$  that consists of the state space  $\mathcal{S}$ , the action space  $\mathcal{A}$ , the discount factor  $\gamma$ , the transition probability of the environment  $\mathbb{P} : \mathcal{S} \times \mathcal{A} \times \mathcal{S} \rightarrow [0, 1]$  and the reward  $r : \mathcal{S} \times \mathcal{A} \rightarrow \mathcal{R}$ . A policy  $\pi$  in RL is a probability distribution on the action  $\mathcal{A}$  over  $\mathcal{S}$ :  $\pi : \mathcal{S} \times \mathcal{A} \rightarrow [0, 1]$ . Given an MDP, our goal is to find a policy  $\pi$  that maximizes the discounted accumulated rewards in this MDP:

$$\max_{\pi} \eta(\pi) = \mathbb{E}_{a_t \sim \pi(\cdot | s_t), s_{t+1} \sim \mathbb{P}(\cdot | s_t, a_t)} \left[ \sum_{t=0}^{\infty} \gamma^t r(s_t, a_t) \right]. \quad (4)$$

Many effective RL algorithms have been developed to find the optimal policy  $\pi$ . In this paper, we use the PPO algorithm. We now briefly review how it works. Given a parameterized policy  $\pi_{\theta}$ , its value function, Q function and advantage function are defined as  $V^{\pi}(s) = \mathbb{E}_{\pi_{\theta}} [\sum_{t=0}^{\infty} \gamma^t r(s_t, a_t) | s_0 = s]$ ,  $Q^{\pi}(s, a) = \mathbb{E}_{\pi_{\theta}} [\sum_{t=0}^{\infty} \gamma^t r(s_t, a_t) | s_0 = s, a_0 = a]$ , and  $A^{\pi}(s, a) = Q^{\pi}(s, a) - V^{\pi}(s)$ , respectively. Given an old policy  $\pi_{\theta_{old}}$ , let  $b_{\theta}(s, a) = \frac{\pi_{\theta}(a|s)}{\pi_{\theta_{old}}(a|s)}$ , PPO optimizes  $\pi_{\theta}$  w.r.t. the following surrogate objective using gradient descent:

$$J^{PPO}(\theta) = \mathbb{E}_{s, a \sim \pi_{\theta_{old}}} \min(b_{\theta}(s, a) A^{\pi_{\theta_{old}}}(s, a), \text{clip}(b_{\theta}(s, a), 1 - \epsilon, 1 + \epsilon) A^{\pi_{\theta_{old}}}(s, a)), \quad (5)$$

where  $\text{clip}(x, a, b) = \max(\min(x, b), a)$ .

### 3.2 MDP Formulation of Personalized Scanning

The CT scanning process is naturally a sequential decision process, where at each time step we need to decide on the measurement angle and the corresponding X-ray dose. Given an Image  $I$  and the number of all possible angles  $N$  (e.g.,  $N = 180$  if we can choose all the integer angles from  $0^{\circ}$  to  $179^{\circ}$ ), we now elaborate how the CT scanning process on  $I$  can be formulated as an MDP:

- 1) The **state** is a sequence  $\vec{s}_t = (s_1, s_2, \dots, s_t)$ , where  $s_t = (p_t, d_t^{\text{ac}}, d_t^{\text{rest}})$ .  $p_t$  is the collected measurement at time step  $t$ .  $d_t^{\text{ac}}$  records the used dose distribution up to time step  $t$ . It is an  $N$  dimensional vector, and the value at each entry represents the used X-ray dose at that corresponding angle. The  $d_t^{\text{rest}}$  is a scalar that represents the amount of the remaining dose that we can use. Because the reconstructed image at time step  $t$  relies on all previously collected measurements, we include all of them in the state.
- 2) The **action** is  $a_t = (a_t^{\text{angle}}, a_t^{\text{dose}})$ .  $a_t^{\text{angle}}$  is the angle we choose at time step  $t$ , and it is a one-hot vector of dimension  $N$ .  $a_t^{\text{dose}} \in [0, 1]$  is the fraction of dose that we apply at the corresponding angle. If at a certain time  $t$ , the total used dose exceeds the total allowed dose, we clip the exceeding dose and terminate the MDP.
- 3) The **reward** is computed as  $r(s_t, a_t) = \text{PSNR}(I_t, I) - \text{PSNR}(I_{t-1}, I)$ , where  $I$  is the groundtruth image, and  $\text{PSNR}(\hat{I}, I)$  represents the Peak Signal to Noise Ratio (PSNR)

value of the reconstructed image  $\hat{I}$ . We use the increment of PSNR to evaluate how much benefit the new chosen angle/dose brings. The reconstructed image  $I_t$  can be obtained from any reconstruction algorithm such as SART, TV-based model, wavelet models, and etc. In this paper, we choose SART as the image reconstruction algorithm for fast computation of reward during training. One may use more refined image reconstruction algorithms. However, this will also significantly increase the training time, and may make it harder to find a better scanning policy.

- 4) The **transition model**  $\mathbb{P}$  represents the scanning process of CT. At time step  $t$ , given the state  $\vec{s}_t$  and action  $a_t$ , the next state  $\vec{s}_{t+1}$  is simply the concatenation of  $\vec{s}_t$  and  $s_{t+1} = (p_{t+1}, d_{t+1}^{\text{ac}}, d_{t+1}^{\text{rest}})$ . We now show how each of the three elements in  $s_{t+1}$  can be computed.
  1. The new measurement is obtained as  $p_{t+1} = p_{t+1}^{\text{true}} + \epsilon$ , where  $p_{t+1}^{\text{true}}$  is the clean projected value obtained using the chosen angle  $a_t^{\text{angle}}$ , and  $\epsilon$  is the measurement noise. The noise depends on the chosen dose  $a_t^{\text{dose}}$  as mentioned in section 2.2:  $\epsilon \sim \mathcal{N}(0, \sigma)$ ,  $\sigma \propto \frac{1}{\sqrt{n_{\max} a_t^{\text{dose}} \exp(-P)}}$ , where  $P$  is the average of  $p_{t+1}^{\text{true}}$ .
  2. The new dose distribution is obtained by adding the new decision:  $d_{t+1}^{\text{ac}} = d_t^{\text{ac}} + \mathbb{1}_{a_t^{\text{angle}}} \cdot a_t^{\text{dose}}$ , where  $\mathbb{1}_{a_t^{\text{angle}}}$  is the one-hot vector of the chosen angle  $a_t^{\text{angle}}$ .
  3. The rest amount of dose is easily computed by subtracting the used dose:  $d_{t+1}^{\text{rest}} = d_t^{\text{rest}} - a_t^{\text{dose}}$ .

The MDP terminates once the dose is used up.

As we choose the increment in PSNR as the reward, the total sum of reward (when there is no discounting, as in our experiments) is the PSNR value of the final reconstructed image. Therefore, if we find the optimal policy to this MDP, it will also have the best reconstruction result for the image.

### 3.3 Policy Network Architecture

Because we include all the previous measurements in the state, the dimension of the state vector increases as we take more measurements. To handle the varying dimensionality of the state vector, we represent the policy network as a Recurrent Neural Network (RNN), so all the information from the past measurements can be encoded in the hidden state of the RNN. Specifically, we use the Gated Recurrent Unit (GRU). Besides, the policy network needs to output two different actions: the discrete action for choosing the angle  $a_t^{\text{angle}}$ , and the continuous action for choosing the dose  $a_t^{\text{dose}}$ . To handle this, we design a special architecture for the policy network, as shown in Figure 1. We use separate Multi-Layer Perceptron (MLP) after the RNN hidden states for these two actions.  $a_t^{\text{angle}}$  is a probability vector of length  $N$ , where the value at each entry represents the probability of choosing that angle. We use Softmax after the final linear layer to obtain the probability vector. We also introduce a mask to remove the previously chosen angles. For the dose usage  $a_t^{\text{dose}}$ , we assume  $a_t^{\text{dose}} \sim \mathcal{N}(\mu^{\text{dose}}, \sigma^{\text{dose}})$ , with the mean and std both learned by a MLP. It is natural to determine the amount of dose after the angle is chosen, i.e.,  $\pi_\theta(a|\vec{s}) = \pi_\theta(a^{\text{dose}}, a^{\text{angle}}|\vec{s}) = \pi_\theta(a^{\text{angle}}|\vec{s})\pi_\theta(a^{\text{dose}}|\vec{s}, a^{\text{angle}})$ , so we concatenate the one-hot vector of the chosen angle as part of the input for the dose MLP.

## 4 Experiments

### 4.1 Experiment Setup

We train the RL policy on 250 CT images of size  $512 \times 512$  from the AAPM dataset of the "2016 NIH-AAPM-Mayo Clinic Low Dose CT Grand Challenge". During training, we use SART as the reconstruction algorithm for computing the reward. The possible angles are all integers in  $[0^\circ, 180^\circ)$ . We use Adam [56] to optimize both the policy network and the value network, with a learning rate of 0.0004, and  $\beta_1, \beta_2 = (0.5, 0.999)$ . More detailed hyperparameters for PPO and network architecture can be found in the code which will be released upon acceptance of this paper.

After training, we test the learned RL policy on another 350 CT images from the AAPM dataset. We compare the following three scanning strategies: (1) **RD-ED**, which selects angles randomly and distributes the dose equally on them; (2) **DS-ED**, which selects angle by a dynamic sample strategy from [42], while distributes the dose equally on them; (3) **RL-AD**: which uses the learned

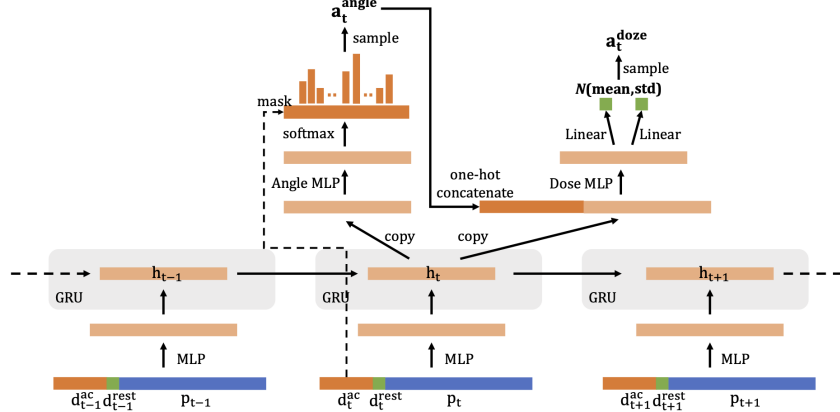


Figure 1: Policy network architecture. Here, each MLP contains two hidden layers with 256 neurons. We use a multi-layer GRU which contains 3 recurrent layers and each layer has 256 neurons. The Angle MLP has one hidden layer of 256 neurons, and the Dose MLP has 2 hidden layers with 256 neurons.

Model	Inference (s)	SART		WF		TV		PD-net	
		PSNR	SSIM	PSNR	SSIM	PSNR	SSIM	PSNR	SSIM
RL-AD	2.50(0.05)	29.22(0.43)	0.683(0.026)	29.77(0.47)	0.723(0.030)	29.52(0.45)	0.702(0.029)	31.12(0.56)	0.800(0.036)
DS-ED	1223.27(279)	28.07(0.45)	0.657(0.027)	28.69(0.48)	0.706(0.033)	28.35(0.46)	0.678(0.030)	30.10(0.60)	0.794(0.027)
RD-ED	2.26(0.04)	27.86(0.47)	0.651(0.026)	28.44(0.48)	0.698(0.031)	28.17(0.46)	0.673(0.030)	29.99(0.69)	0.789(0.028)

Table 1: First column presents the mean (std) of inference time for each CT image by the compared three methods among all 350 testing CT images. The rest shows the mean (std) of the PSNR and SSIM of the reconstructed images using different reconstruction algorithms.

personalized policy for both angle selection and dose allocation at each chosen angle. To shorten the inference time for DS-ED, we first use uniform samples with  $10^\circ$  spacing and then use information gain to decide the rest of the angles. During testing, we use four different reconstruction algorithms: SART, TV regularization (TV) [11, 57], wavelet frame (WF) regularization [58, 7], and the recently proposed deep learning method PD-net [59]. The evaluation metric is PSNR and the structure similarity metric (SSIM) of the reconstructed images.

A difficulty in conducting a fair comparison of RD-ED with DS-ED and RL-AD is that the number of selected angles of DS-ED and RL-AD can be different for different subjects (see Figure 3). In our experiments below, we choose the number of measurement angles for RD-ED to be 53, which is the mean number of measurement angles selected by RL-AD over all the 350 test images. Thus, the dose on each measurement angle of RD-ED is  $1/53$ . We also note that the deep reconstruction model PD-net is trained from scratch on the 250 images in the training set using 53 angles and parallel beams geometry.

## 4.2 Results

Table 1 presents the mean and standard deviation of the PSNR and SSIM values of the reconstructed images of all compared scanning strategies and reconstruction algorithms. As one can see that the proposed scanning strategy RL-AD significantly outperforms dynamic sampling (DS-ED) and random scanning (RD-ED), while DS-ED outperforms RD-ED. Furthermore, we present the inference time for each of the compared scanning strategy. The inference time includes the time to compute measurements. Since DS-ED needs to frequently reconstruct CT image during the decision on measurement angles, it is significantly slower than RL-AD and RD-ED.

We also note that the RL-policy is trained only using the SART for computing the reward function, whereas the learned policy can generalize well to three other reconstruction algorithms, i.e., the TV regularization, the wavelet frame regularization and the deep learning model PD-net, where it still brings a notable improvement upon the dynamic sampling and random scanning baseline in reconstruction quality.

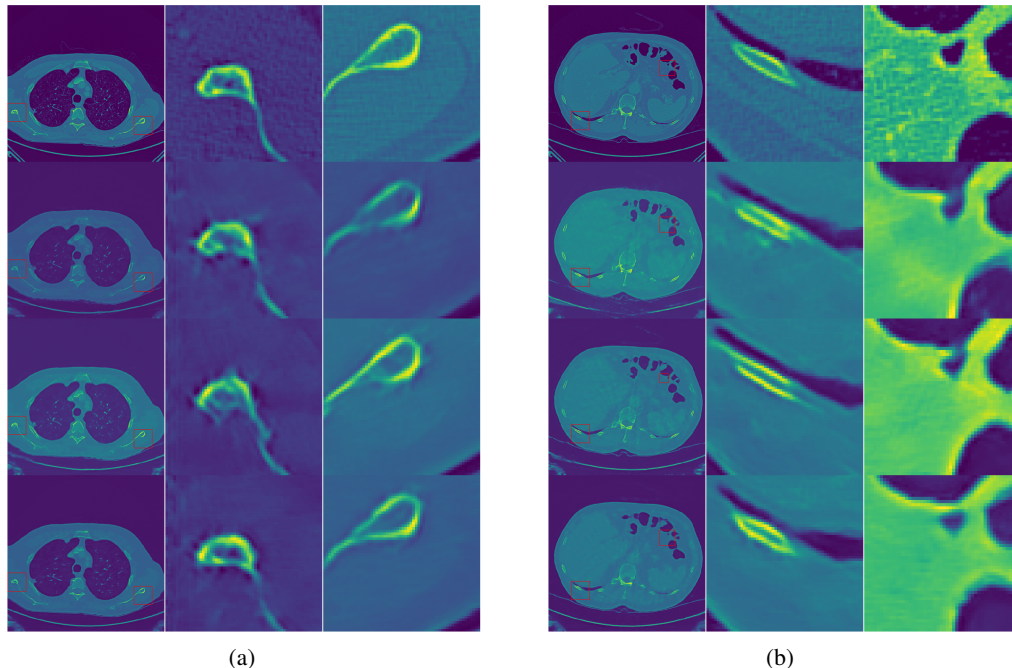


Figure 2: Two examples of the reconstructed images. The top row contains the ground truth images and their zoom-in views. The second through the fourth row contain results from RD-ED, DS-ED and RL-AD respectively, and combined with PD-net’s reconstruction. Note that RL-AD selects 64 measurement angles for the subject in (a) and 45 measurement angles for the subject in (b), and with adaptive dose.

In Figure 2, we further show two examples of the reconstructed images using the random scanning strategy (RD-ED), the dynamic sampling strategy (DS-ED) and the learned personalized policy (RL-AD), reconstructed using the deep learning model PD-net. We can see that the reconstructions using the RL policy are of higher qualities than those using random and dynamic sampling strategy, especially from the zoom-in views of the figures.

We plot the distribution of number of measurements taken by the learned personalized policy (RL-AD) in Figure 3 (a). The result demonstrates that for different subjects, the learned RL policy selects different number of angles and dose allocations. In Figure 3 (b), (c) and (d), we take 8 images on which the learned RL policy selects 45, 54 and 64 angles respectively and plot the distributions of the dose usage of these images. It can be seen that images using the same number of measurement angles have very similar dose allocations, and images that have more measurement angles use less dose at each angle. In Figure 4, we show 3 example images where the RL policy selects 45, 54 and 63 measurement angles respectively. We can see that images upon which the RL policy selects more measurement angles have more structures in the image, and thus more information/measurements need to be collected to obtain a high-quality reconstruction. In Figure 5, we present the selected angles and part of the dose allocation on the subjects shown in Figure 4.

## 5 Conclusion

In this paper, we proposed to use reinforcement learning to learn a personalized CT scanning strategy for measurement angle selection and dose allocation. We formulated the CT scanning process as a Markov Decision Process, and used the PPO algorithm to solve it. After training on 250 real 2D CT images, we validated the learned personalized scanning policy on another 350 CT images. Our validation showed that the personalized scanning policy lead to better overall reconstruction results in terms of PSNR values, and generalized well to be combined with different reconstruction algorithms. We also demonstrated that the personalized policy can indeed adjust its angle selection and dose allocations adaptive to different subjects. One drawback of the proposed method is the long training

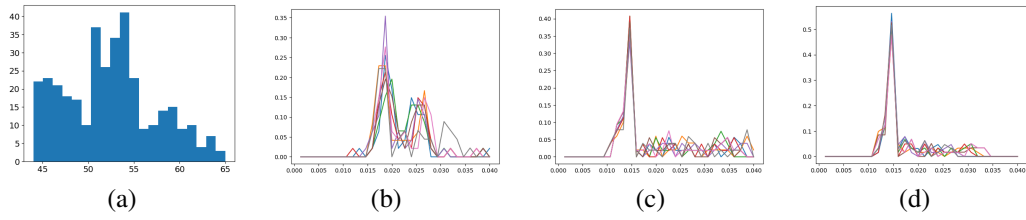


Figure 3: (a) Distribution of number of measurements of the learned policy (RL-AD) on all the 350 testing CT images. (b) Dose usage distribution of 8 images that use around 45 measurements. (c) Dose usage distribution of 8 images that use around 54 measurements. (d) Dose usage distribution of 8 images that use around 64 measurements.

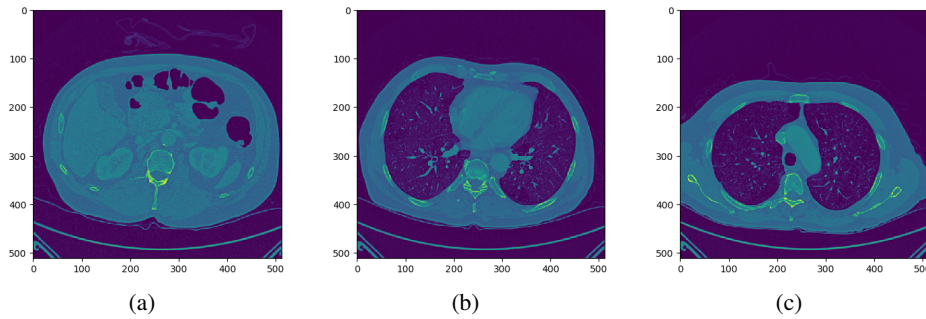


Figure 4: (a): an example image that takes 45 measurements. (b): an example image that takes 54 measurements. (c): an example image that takes 64 measurements. We can see that the images for which RL selects more measurement angles contains more structures.

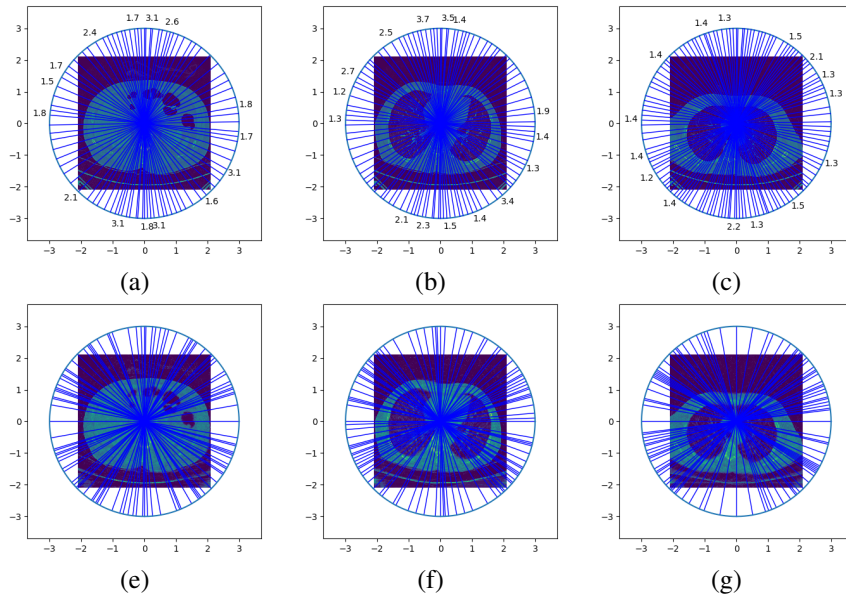


Figure 5: The angle selection and part of the dose allocations of the CT image in Figure 4.



time (approximately 24 hours) even for 2D images, because RL algorithms usually need lots of simulation samples to converge, and to compute the reward in our formulated MDP requires running a reconstruction algorithm at each time step. This might prohibits the application of our method to 3D cases.

## 6 Broader Impact

As shown by our experiments, the learned personalized scanning strategy significantly improves the reconstruction quality. We hope our work can draw more attention on how to design more efficient and effective CT scanning strategies using latest tools developed in machine learning. Our method may also be generalized to other imaging modality such as Magnetic Resonance Imaging (MRI), where a smart scanning strategy may significantly reducing acquisition time which has been one of the major challenge for MRI. There are also some potential issues of our proposed method: 1) The training algorithm of the proposed framework can be difficult to tune; 2) The design of the MDP greatly affects the final performance and it is currently way under-explored; 3) In our training, we adopt an idealize assumption that the linear operator  $A$  and the noise  $\epsilon$  is a close approximation to the real physics of the imaging system, which make cause problem when deploying the trained RL policy to real imaging systems.

## Acknowledgments and Disclosure of Funding

Bin Dong is supported in part by National Natural Science Foundation of China (NSFC) grant No. 11831002, Beijing Natural Science Foundation (No. 180001) and Beijing Academy of Artificial Intelligence (BAAI).

## References

- [1] Alexander Katsevich. Theoretically exact filtered backprojection-type inversion algorithm for spiral ct. *Siam Journal on Applied Mathematics*, 62(6):2012–2026, 2002.
- [2] R. Gordon, R. Benderab, and G. T. Herman. Algebraic reconstruction techniques (art) for three-dimensional electron microscopy and x-ray photography. *Journal of Theoretical Biology*, 1970.
- [3] D. Donoho. Compressed sensing. *IEEE Transactions on Information Theory*, 52(4):1289–1306, 2006.
- [4] Emmanuel J. Candes, Yonina C. Eldar, et al. Compressed sensing with coherent and redundant dictionaries. 2010.
- [5] T. Goldstein and S. Osher. The split bregman method for l1-regularized problems. *SIAM J. Imaging Sci.*, 2(2):323–343, 2009.
- [6] S. Boyd, N. Parikh, et al. Distributed optimization and statistical learning via the alternating direction method of multipliers. *Found. Trends Mach. Learn.*, 3(1):1–122, 2011.
- [7] Jian-Feng Cai, Stanley Osher, and Zuwei Shen. Split bregman methods and frame based image restoration. *Multiscale Model. Simul.*, 8(2):337–369, 2009.
- [8] Antonin Chambolle and Thomas Pock. A first-order primal-dual algorithm for convex problems with applications to imaging. *J. Math. Imaging Vis.*, 40(1):120–145, 2011.
- [9] Mingqiang Zhu and Tony Chan. An efficient primal-dual hybrid gradient algorithm for total variation image restoration. *UCLA CAM Report*, 2008.
- [10] Ernie Esser, Xiaoqun Zhang, et al. A general framework for a class of first order primal-dual algorithms for convex optimization in imaging science. *SIAM J. Imaging Sci.*, 3(4):1015–1046, 22010.
- [11] Leonid I. Rudin, Stanley Osher, and Emad Fatemi. Nonlinear total variation based noise removal algorithms. *Physica D: nonlinear phenomena*, 60(1-4):259–268, 1992.
- [12] Antoni Buades, Bartomeu Coll, and J-M Morel. A non-local algorithm for image denoising. In *2005 IEEE Computer Society Conference on Computer Vision and Pattern Recognition (CVPR'05)*, volume 2, pages 60–65. IEEE, 2005.
- [13] Kostadin Dabov, Alessandro Foi, Vladimir Katkovnik, and Karen Egiazarian. Image denoising by sparse 3-d transform-domain collaborative filtering. *IEEE Transactions on image processing*, 16(8):2080–2095, 2007.

- [14] Shuhang Gu, Lei Zhang, Wangmeng Zuo, and Xiangchu Feng. Weighted nuclear norm minimization with application to image denoising. In *Proceedings of the IEEE conference on computer vision and pattern recognition*, pages 2862–2869, 2014.
- [15] Ingrid Daubechies. *Ten lectures on wavelets*, volume 61. Siam, 1992.
- [16] Stéphane Mallat. *A wavelet tour of signal processing*. Elsevier, 1999.
- [17] Bin Dong, Zuowei Shen, et al. Mra based wavelet frames and applications. *IAS Lecture Notes Series, Summer Program on “The Mathematics of Image Processing”*, Park City Mathematics Institute, 19, 2010.
- [18] Michael Elad and Michal Aharon. Image denoising via sparse and redundant representations over learned dictionaries. *IEEE Transactions on Image processing*, 15(12):3736–3745, 2006.
- [19] Jian-Feng Cai, Hui Ji, Zuowei Shen, and Gui-Bo Ye. Data-driven tight frame construction and image denoising. *Applied and Computational Harmonic Analysis*, 37(1):89–105, 2014.
- [20] Cheng Tai and E Weinan. Multiscale adaptive representation of signals: I. the basic framework. *The Journal of Machine Learning Research*, 17(1):4875–4912, 2016.
- [21] Stanley Osher, Zuoqiang Shi, and Wei Zhu. Low dimensional manifold model for image processing. *SIAM Journal on Imaging Sciences*, 10(4):1669–1690, 2017.
- [22] Ge Wang. A perspective on deep imaging. *Ieee Access*, 4:8914–8924, 2016.
- [23] Ge Wang, Mannudeep Kalra, and Colin G Orton. Machine learning will transform radiology significantly within the next 5 years. *Medical physics*, 44(6):2041–2044, 2017.
- [24] Michael T McCann, Kyong Hwan Jin, and Michael Unser. Convolutional neural networks for inverse problems in imaging: A review. *IEEE Signal Processing Magazine*, 34(6):85–95, 2017.
- [25] Ge Wang, Jong Chu Ye, Klaus Mueller, and Jeffrey A Fessler. Image reconstruction is a new frontier of machine learning. *IEEE transactions on medical imaging*, 37(6):1289–1296, 2018.
- [26] Hai-Miao Zhang and Bin Dong. A review on deep learning in medical image reconstruction. *Journal of the Operations Research Society of China*, pages 1–30, 2020.
- [27] Hu Chen, Yi Zhang, Mannudeep K Kalra, Feng Lin, Yang Chen, Peixi Liao, Jiliu Zhou, and Ge Wang. Low-dose ct with a residual encoder-decoder convolutional neural network. *IEEE transactions on medical imaging*, 36(12):2524–2535, 2017.
- [28] Kyong Hwan Jin, Michael T McCann, Emmanuel Froustey, and Michael Unser. Deep convolutional neural network for inverse problems in imaging. *IEEE Transactions on Image Processing*, 26(9):4509–4522, 2017.
- [29] Eunhee Kang, Junhong Min, and Jong Chul Ye. A deep convolutional neural network using directional wavelets for low-dose x-ray ct reconstruction. *Medical physics*, 44(10):e360–e375, 2017.
- [30] Zhicheng Zhang, Xiaokun Liang, Xu Dong, Yaoqin Xie, and Guohua Cao. A sparse-view ct reconstruction method based on combination of densenet and deconvolution. *IEEE transactions on medical imaging*, 37(6):1407–1417, 2018.
- [31] Qingsong Yang, Pingkun Yan, Yanbo Zhang, Hengyong Yu, Yongyi Shi, Xuanqin Mou, Mannudeep K Kalra, Yi Zhang, Ling Sun, and Ge Wang. Low-dose ct image denoising using a generative adversarial network with wasserstein distance and perceptual loss. *IEEE transactions on medical imaging*, 37(6):1348–1357, 2018.
- [32] E. J. Candes, J. Romberg, and T. Tao. Robust uncertainty principles: Exact signal reconstruction from highly incomplete fourier information. *IEEE Trans. Info. Theory*, 52(2), 2006.
- [33] Burr Settles. Active learning literature survey. Technical report, University of Wisconsin-Madison Department of Computer Sciences, 2009.
- [34] Yuxi Li. Deep reinforcement learning: An overview. *arXiv:1701.07274*, 2017.
- [35] Ryutarou Ohbuchi and Masaki Aono. Quasi-monte carlo rendering with adaptive sampling. 1996.
- [36] K.A.Mohan, S.V.Venkatakrishnan, E.B.Gulsoy J.W.Gibbs, X.Xiao, M. D. Graef, P. W. Voorhees, and C. A. Bouman. Timbir: A method for time-space reconstruction from interlaced views. *IEEE Transactions on Computational Imaging*, pages 96–111, 2015.
- [37] K. Mueller. Selection of optimal views for computed tomography reconstruction. *Patent WO*, Jan. 28 2011.
- [38] Z.Wang and G.R.Arce. Variable density compressed image sampling. *Image Processing, IEEE Transactions*, 19(1):264–270, 2010.
- [39] Shihao Ji, Ya Xue, and Lawrence Carin. Bayesian compressive sensing. *IEEE Transactions on Signal Processing*, 56(6):2346–2356, 2008.
- [40] Matthias W Seeger and Hannes Nickisch. Compressed sensing and bayesian experimental design. In *Proceedings of the 25th international conference on Machine learning*, pages 912–919, 2008.

- [41] K Joost Batenburg, Willem Jan Palenstijn, Péter Balázs, and Jan Sijbers. Dynamic angle selection in binary tomography. *Computer Vision and Image Understanding*, 117(4):306–318, 2013.
- [42] Andrei Dabrovolski, Kees Joost Batenburg, and Jan Sijbers. Dynamic angle selection in x-ray computed tomography. *Nuclear Instruments and Methods in Physics Research Section B: Beam Interactions with Materials and Atoms*, 324:17–24, April 2014.
- [43] Andrei Dabrovolski, Kees Joost Batenburg, and Jan Sijbers. Dynamic angle selection in x-ray computed tomography. *Nuclear Instruments and Methods in Physics Research Section B: Beam Interactions with Materials and Atoms*, 324:17–24, 2014.
- [44] G. D. Godaliyadda, M. A. Uchic D. Hye Ye, M. A. Groeber, G. T. Buzzard, and C. A. Bouman. A supervised learning approach for dynamic sampling. *S&T Imaging. International Society for Optics and Photonics*, 2016.
- [45] G. M. Dilshan P. Godaliyadda, Dong Hye Ye, Michael D. Uchic, Michael A. Groeber, Gregory T. Buzzard, and Charles A. Bouman. A framework for dynamic image sampling based on supervised learning (slads). *arXiv:1703.04653*, 2017.
- [46] Yan Zhang, G. M. Dilshan Godaliyadda, Nicola Ferrier, Emine B. Gulsoy, Charles A. Bouman, and Charudatta Phatak. Slads-net: Supervised learning approach for dynamic sampling using deep neural networks. *Electronic Imaging, Computational Imaging XVI*, 2018.
- [47] Shijie Zhang, Zhengtian Song, GM Dilshan P Godaliyadda, Dong Hye Ye, Azhad U Chowdhury, Atanu Sengupta, Gregory T Buzzard, Charles A Bouman, and Garth J Simpson. Dynamic sparse sampling for confocal raman microscopy. *Analytical chemistry*, 90(7):4461–4469, 2018.
- [48] Abderrahim Halimi, Philippe Ciuciu, Aongus Mccarthy, Stephen Mclaughlin, and Gerald Buller. Fast adaptive scene sampling for single-photon 3d lidar images. *IEEE CAMSAP 2019 - International Workshop on Computational Advances in Multi-Sensor Adaptive Processing*, Dec. 2019.
- [49] Etienne Monier, Nathalie Brun Thomas Oberlin, Xiaoyan Li, Marcel Tenc, and Nicolas Dobigeon . Fast reconstruction of atomic-scale stem-eels images from sparse sampling. *Ultramicroscopy*, 2020.
- [50] Jeffrey M. Ede. Adaptive partial scanning transmission electron microscopy with reinforcement learning. *arXiv:2004.02786*.
- [51] K. Mueller, R. Yagel, and J.J. Wheller. Anti-aliased three-dimensional cone-beam reconstruction of low-contrast objects with algebraic methods. *IEEE Transactions On Medical Imaging*, 6(18):519–537, 1999.
- [52] Emil Y Sidky and Xiaochuan Pan. Image reconstruction in circular cone-beam computed tomography by constrained, total-variation minimization. *Physics in medicine and biology*, 53:4777, 2008.
- [53] Bin Dong, Jia Li, and Zuowei Shen. X-ray ct image reconstruction via wavelet frame based regularization and radon domain inpainting. *Journal of Scientific Computing*, 54(2-3):333–349, 2013.
- [54] Lifeng Yu, Maria Shiung, Dayna Jondal, and Cynthia H McCollough. Development and validation of a practical lower-dose-simulation tool for optimizing computed tomography scan protocols. *Journal of Computer Assisted Tomography*, 36(4):477–487, July 2012.
- [55] J. Schulman and F. Wolski. Proximal policy optimization algorithms. *arXiv:1707.06347v2*, 2017.
- [56] Diederik P. Kingma and Jimmy Ba. Adam: A method for stochastic optimization. *arXiv:1412.6980*, 2014.
- [57] Tom Goldstein and Stanley Osher. The split bregman method for  $l_1$ -regularized problems. *SIAM J. Imaging Sci.*, 2(2):323–343, 2009.
- [58] Amos Ron and Zuowei Shen. Affine systems in  $L_2(\mathbb{R}^d)$ : The analysis of the analysis operator. *J. Funct. Anal.*, 148(2):408–447, 1997.
- [59] Jonas Adler and Ozan Oktem. Learned primal-dual reconstruction. *IEEE Trans. Med. Imag- ing*, 37(6):1322–1332, 2018.